Nanoscale Horizons

ROYAL SOCIETY OF CHEMISTRY

COMMUNICATION

View Article Online
View Journal | View Issue

Cite this: *Nanoscale Horiz.*, 2022, 7, 1404

Received 5th July 2022,
Accepted 17th August 2022

DOI: 10.1039/d2nh00318j

rsc.li/nanoscale-horizons

Strain-mediated oxygen evolution reaction on magnetic two-dimensional monolayers†

Mingjie Pu, Yufeng Guo* and Wanlin Guo*

By screening 56 magnetic 2D monolayers through first-principles calculations, it was found that 8 magnetic 2D monolayers (CoO_2, FeO_2, FeSe, FeTe, VS_2, VSe_2, VTe_2 and $CrSe_2$) can bind O*, OH* and OOH* intermediates of the oxygen evolution reaction (OER), in which the overpotentials of CoO_2, FeO_2, VSe_2, and VTe_2 monolayers are 0.684, 1.107, 0.863 and 0.837 V, respectively. After applying suitable biaxial tensile strains, the overpotentials of CoO_2, FeO_2 and VTe_2 monolayers are reduced over 40%. In particular, the overpotentials of CoO_2 and VTe_2 monolayers decrease to 0.372 V and 0.491 V under the biaxial tensile strains of 4.0% and 3.0%, respectively, which are comparable to the reported overpotentials of noble metal and low-dimensional materials. Tensile strains modify the potential determining step for the OER and enhance the catalytic activity of metal atoms of magnetic 2D monolayers. Magnetic 2D monolayers could be activated by strain engineering as catalysts for the OER.

New concepts

Using two-dimensional (2D) materials as catalysts to improve the chemical reaction activity and efficiency has attracted great scientific interest and attention. The oxygen evolution reaction (OER) plays an important role in sustainable and renewable energy-conversion and -storage technologies. However, the catalytic capability of the basal surfaces of magnetic 2D materials for the OER has seldom been considered. Here, by screening 56 predicted magnetic 2D monolayers through extensive first-principles calculations we show that 8 magnetic 2D monolayers (CoO_2, FeO_2, FeSe, FeTe, VS_2, VSe_2, VTe_2 and $CrSe_2$) can bind O*, OH* and OOH* intermediates that are key reaction steps in the OER. After applying suitable biaxial tensile strain values, the overpotentials of the CoO_2, FeO_2 and VTe_2 monolayers are reduced over 40%. In particular, the overpotentials of CoO_2 and VTe_2 monolayers decrease to 0.372 V and 0.491 V under biaxial tensile strain values of 4.0% and 3.0%, respectively, which are comparable to the reported overpotentials of noble metal and low-dimensional materials. Tensile strain modifies the potential determining step of the OER and significantly enhances the catalytic activity of the metal atoms of magnetic 2D monolayers. Our results highlight a possible route for utilizing strain engineering to activate magnetic 2D monolayers as catalysts for the OER.

Introduction

Sustainable and renewable energy-conversion and -storage technologies, including electrocatalytic water splitting,[1] fuel cells[2] and metal–air batteries,[3] have been widely applied in clean and green energy fields.[4–6] The oxygen evolution reaction (OER) plays an important role in enabling the chemical process and efficiency in those energy-storage technologies.[7,8] The multi-step proton-coupled electron-transfer process in the OER usually leads to a high overpotential and sluggish reaction kinetics.[9] Traditional noble metal catalysts like IrO_2[10] and RuO_2[11,12] have state-of-the-art chemical activity for improving the efficiency of the OER, but noble metal elements and their compounds are rare in the Earth, which results in high exploitation costs and limits their widespread application. Therefore, seeking low-cost, stable and high-efficiency catalysts is critical for the OER and the development of green and clean energy-storage technologies.

In recent years, graphene and transition metal dichalcogenides (TMDs) as typical two-dimensional (2D) van der Waals (vdW) materials have exhibited excellent chemical properties,[13,14] and can be good catalysts for water splitting[15–17] and the hydrogen evolution reaction (HER).[18–20] For the OER, the adsorption capability of O*, OH* and OOH* intermediates that are critical reaction steps of the OER is different on perfect graphene[21] and

State Key Laboratory of Mechanics and Control of Mechanical Structures, MOE Key Laboratory for Intelligent Nano Materials and Devices, College of Aerospace Engineering, Nanjing University of Aeronautics and Astronautics, Nanjing, 210016, China. E-mail: yfguo@nuaa.edu.cn, wlguo@nuaa.edu.cn

† Electronic supplementary information (ESI) available: 56 easily exfoliated magnetic 2D monolayers, table of overpotentials of 8 magnetic 2D monolayers for the OER without strain and under the optimal biaxial tensile strains, the Gibbs free energies of adsorbed intermediates on FeO_2, VSe_2 and VTe_2 monolayers under different biaxial tensile strains, the variations of G_{OH^*} with G_{O^*} or G_{OOH^*} for FeO_2, VSe_2 and VTe_2, the DOS of non-metal atoms (O, Se and Te) for CoO_2, FeO_2, VSe_2 and Vte_2 under different biaxial tensile strains, and the overpotentials of CoO_2 and Vte_2 under uniaxial tensile strains, the overpotentials by the PBE+*U* method, and the results of non-magnetic 2D monolayers. See DOI: https://doi.org/10.1039/d2nh00318j

TMDs.[22] The relatively high adsorption energies of the intermediates give rise to higher overpotentials in the OER on the basal planes of graphene[23] and TMDs.[24] Further experimental and theoretical studies have shown that the adsorption sites and energies of the O*, OH* and OOH* intermediates can be altered and controlled by introducing defects or single-atom metals such as Fe, Co, Mn or Ni on the graphene and TMDs surfaces, upon which the OER overpotentials are decreased accordingly.[25] For example, the electrochemical overpotential of mononuclear Mn embedded in nitrogen-doped graphene is only 0.337 V, which is better than traditional noble metal catalysts.[26] Using structural engineering or combining active single-atom metals, 2D vdW materials could play the role of a catalyst in enhancing the OER.[27,28] Except from non-magnetic 2D materials, magnetic 2D materials have been successfully obtained and have also attracted a great deal of scientific attention and interest because of their potential spintronics and valleytronics applications.[29] The heterostructures formed by magnetic 2D materials show good catalytic activity for the OER.[30–32] Different from experimental synthesis and exfoliation for achieving magnetic 2D materials,[33,34] a recent theoretical study based on high-throughput computation predicted 56 possible magnetic 2D materials that are held by weak vdW interactions in their bulk states.[35] Magnetic 2D materials possess a flat atomic structure and a high surface-to-volume ratio, making an ideal platform for catalytic reactions.[36] On the other hand, mechanical deformation and loading have been proved to be an effective way to change and improve the chemical properties of 2D materials, which can also render 2D materials with novel physical effects.[37] However, the OER on the basal surfaces of magnetic 2D materials and the influence of mechanical deformation on the catalytic activity of magnetic 2D materials have seldom been investigated.

In this study, 56 magnetic 2D monolayers that were theoretically predicted are considered as possible OER catalysts *via* first-principles calculations. Our calculation results show that O*, OH* and OOH* intermediates can only adsorb on the basal surfaces of 8 magnetic 2D monolayers, in which the overpotentials of the CoO_2, FeO_2, VSe_2, and VTe_2 monolayers for the OER are 0.684, 1.107, 0.863 and 0.837 V, respectively. When the biaxial tensile strain of 4.0%, 6.0%, 5.0% and 3.0% is applied on the CoO_2, FeO_2, VSe_2 and VTe_2 monolayers, their overpotentials decrease to the lowest values of 0.372, 0.600, 0.796 and 0.491 V, respectively. For the CoO_2 monolayer, the overpotential of 0.372 V is comparable to that of the noble metal catalyst RuO_2. The biaxial tensile strain changes the potential determining step (PDS) of the OER, strengthens the adsorption of intermediates on the 2D monolayers and reduces the energy barriers of intermediate transition. Strain engineering can enhance the chemical activity of magnetic 2D monolayers, which makes them suitable as catalysts in the OER.

Model and method

According to theoretical prediction and experimental results,[35,38,39] 56 magnetic 2D monolayers were considered (see Table S1 in the ESI†) and constructed in rectangular unit cells, the lengths of which in the x and y directions are both larger than 15 Å. In Fig. 1, the atomic structures of three 2D monolayers are given. The periodic boundary conditions were applied in the x and y directions and the vacuum regions were set as 20 Å in the z direction. The O*, OH* and OOH* intermediates that are involved in the OER adsorb on the center of basal surfaces. All spin-polarized calculations were performed within the framework of density functional theory (DFT) as implemented in the Vienna *ab initio* simulation package (VASP) using the projector augmented wave method with the generalized gradient approximation (GGA) in the Perdew–Burke–Ernzerhof (PBE) exchange–correlation functional.[40–42] The influence of van der Waals interactions was considered using DFT-D3 correction, which was developed by Grimme *et al.*[43] The plane wave energy cutoff was set to 500 eV and the special Γ-centered k points sampled on a $3 \times 3 \times 1$ mesh were employed after the convergence test. Biaxial tensile strain was applied by gradually increasing the unit cell lengths in the x and y directions. Then those systems were relaxed using a conjugate-gradient algorithm until the force on each atom was less than 0.01 eV $Å^{-1}$.

In the electrochemical reaction, the overall OER can be written as:[44]

$$2H_2O(l) \rightarrow O_2(g) + 4H^+ + 4e^- \quad (1)$$

The overall reaction involves four elementary reaction steps, and each step involves the transfer of one electron. The specific expressions are as follows:[44]

$$H_2O(l) + * \rightarrow OH^* + H^+ + e^- \quad (2a)$$

$$OH^* \rightarrow O^* + H^+ + e^- \quad (2b)$$

$$O^* + H_2O(l) \rightarrow OOH^* + H^+ + e^- \quad (2c)$$

$$OOH^* \rightarrow * + O_2(g) + H^+ + e^- \quad (2d)$$

where * represents an active site on the basal surface of the magnetic 2D monolayers. $H_2O(l)$ and $O_2(g)$ are a liquid-phase water molecule and a gas-phase oxygen molecule, respectively, and O*, OH* and OOH* are the three different adsorbed intermediates in the OER. H^+ and e^- are a proton and electron, respectively.

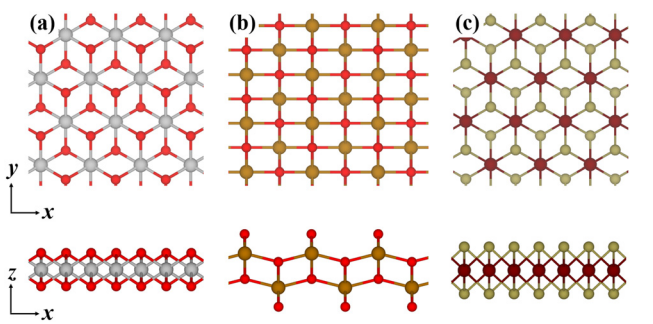

Fig. 1 Top (upper) and side (lower) views of the atomic configurations of three magnetic 2D monolayers: (a) CoO_2, (b) FeO_2, and (c) VTe_2.

The binding energies of different adsorbed intermediates are calculated using the following equations:[45]

$$\Delta E_{OH^*} = E_{slab+OH^*} - E_{slab} - \left(E_{H_2O} - \frac{1}{2}E_{H_2}\right) \quad (3a)$$

$$\Delta E_{O^*} = E_{slab+O^*} - E_{slab} - \left(E_{H_2O} - E_{H_2}\right) \quad (3b)$$

$$\Delta E_{OOH^*} = E_{slab+OOH^*} - E_{slab} - \left(2E_{H_2O} - \frac{3}{2}E_{H_2}\right)$$

where ΔE_{OH^*}, ΔE_{O^*} and ΔE_{OOH^*} are the binding energies of the OH*, O* and OOH* intermediates, respectively. E_{slab} is the ground-state energy of the magnetic 2D monolayer. $E_{slab+OH^*}$, E_{slab+O^*} and $E_{slab+OOH^*}$ are the total energies of the magnetic 2D monolayer binding with the OH*, O* and OOH* intermediates, respectively. E_{H_2O} and E_{H_2} are the energies of H_2O and H_2 molecules in the liquid and gas phase, respectively.

At zero electrode potential and pH = 0, the Gibbs free energy of the adsorbed intermediates is obtained using the following equation:[45]

$$G_{ads} = \Delta E_{ads} + \Delta E_{ZPE} - T\Delta S \quad (4)$$

where ΔE_{ads} is the binding energy, ΔE_{ZPE} is the difference in zero point vibrational energy, T is the thermodynamic temperature (298.15 K), and ΔS is the change in entropy of the intermediates adsorbed on the magnetic 2D monolayer at one standard atmospheric pressure (101.325 kPa).

For each elementary reaction step, the Gibbs free energy difference $\Delta G_i (i = 1, 2, 3, 4)$ is given by these equations:[45,46]

$$\Delta G_1 = G_{OH^*} \quad (5a)$$

$$\Delta G_2 = G_{O^*} - G_{OH^*} \quad (5b)$$

$$\Delta G_3 = G_{OOH^*} - G_{O^*} \quad (5c)$$

$$\Delta G_4 = 4.92 - G_{OOH^*} \quad (5d)$$

where the value of 4.92 eV is the total change in the Gibbs free energy for the overall reaction $2H_2O \rightarrow O_2 + 2H_2$ at 298.15 K. After that, the theoretical overpotential η for the OER is obtained using:[45]

$$\Delta G_i^{max} = \max[\Delta G_1, \Delta G_2, \Delta G_3, \Delta G_4] \quad (6)$$

$$\eta = \Delta G_i^{max}/e - 1.23 \quad (7)$$

In the OER, the PDS is an important reaction step that dominates the overall catalytic performance of catalysts,[47] which can be obtained from ΔG_i^{max}.

Results and discussion

The OER includes four elementary steps in which oxygen-containing intermediates (O*, OH* and OOH*) adsorb on the surfaces of magnetic 2D monolayers. After screening the 56 magnetic 2D monolayers *via* first-principles calculations, eight magnetic 2D monolayers on which all the intermediates can adsorb were selected, and they are CoO_2, FeO_2, FeSe, FeTe, VS_2, VSe_2, VTe_2 and $CrSe_2$. The Gibbs free energy differences ΔG_i and overpotentials η of the eight monolayers for the OER were calculated according to eqn (5)–(7). For the 8 magnetic 2D monolayers, monolayer CoO_2 possesses the lowest overpotential of 0.684 V, see Table S2 in the ESI.† An ideal catalyst for the OER is one in which all Gibbs free energy differences between two adjacent elementary reactions are 0 eV at 1.23 V external potential, and a lower overpotential means a better catalytic capability. In order to improve the catalytic properties for the OER, in-plane biaxial tensile strain was applied on the eight magnetic 2D monolayers. Our results show that the overpotential of monolayer CoO_2 decreases from 0.684 V to the lowest value of 0.372 V when a 4.0% biaxial tensile strain ε_{xy} was applied, which is close to that of RuO_2.[44] Meanwhile, the overpotentials of monolayer FeO_2, VSe_2 and VTe_2 decrease to the lowest values of 0.600, 0.796 and 0.491 V when 6.0%, 5.0% and 3.0% biaxial tensile strain ε_{xy} is applied, respectively. For the other four magnetic monolayers, their overpotentials are all larger than 1 V, even in the presence of tensile strain, see Table S2 (ESI†). Reduction of the overpotential demonstrates the validity of tensile strain in enhancing the catalytic performance of magnetic 2D materials for the OER. Moreover, Table 1 shows a comparison of the overpotentials of magnetic 2D materials for the OER with other low-dimensional materials. The overpotentials of 0.372 V for the strained CoO_2 monolayer and 0.491 V for the strained VTe_2 monolayer are comparable to the theoretically predicted overpotentials of non-magnetic nanomaterials and nanostructures. This means that magnetic 2D CoO_2 and VTe_2 combined with strain engineering can be used as catalysts for the OER on their basal planes.

Fig. 2(a) shows the Gibbs free energy diagram of the adsorbed intermediates on monolayer CoO_2 for the OER. The PDS of the OER on monolayer CoO_2 without strain is the first step ΔG_1 ($H_2O \rightarrow$ *OH) with a value of 1.914 eV, but the PDS changes to the second step ΔG_2 (*OH $\rightarrow$ *O) and decreases to 1.602 eV under a biaxial tensile strain of 4.0%, as shown in Fig. 2(a). By contrast, it can be seen from Fig. 2(b) that the PDSs of monolayer FeO_2, VSe_2 and VTe_2 under biaxial tensile strain values of 6.0%, 5.0% and 3.0%, respectively, are all the third step ΔG_3 (*O $\rightarrow$ *OOH). To further elucidate the effect of tensile deformation on the PDS, the variation in the Gibbs free energy difference (ΔG_i) of the four magnetic 2D monolayers with biaxial tensile strain are shown in Fig. 3. Excluding 4.0% biaxial

Table 1 Theoretical predicted overpotentials for the OER using low-dimensional materials as catalysts

Material	Overpotential (V)	Ref.
2D-CoO_2 (4.0% ε_{xy})	0.372	This work
2D-VTe_2 (3.0% ε_{xy})	0.491	This work
Fe–MoS_2 nanosheets	0.328	28
Mn-NG	0.337	26
RuO_2 (110)	0.370	44
Zn@$MoSi_2N_4$	0.380	48
Armchair N-doped graphene	0.405	49
Ni-NHGF	0.420	25
Pd-GeC	0.440	50
Pt-MoS_2 edge	0.460	51

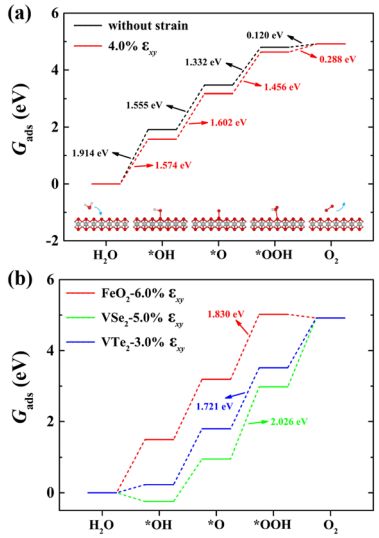

Fig. 2 Gibbs free energy diagrams of the adsorbed intermediates for the OER on (a) monolayer CoO_2 without strain and under 4.0% biaxial tensile strain, and (b) monolayer FeO_2, VSe_2 or VTe_2 under 6.0%, 5.0% and 3.0% biaxial tensile strain, respectively. The inset in (a) shows the reaction steps in which the O*, OH* and OOH* intermediates adsorb on monolayer CoO_2, where the red, gray and white spheres denoted O, Co and H atoms, respectively.

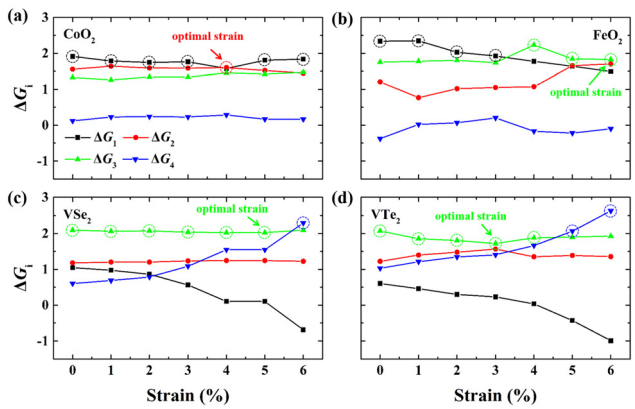

Fig. 3 Gibbs free energy differences (ΔG_i) in the elementary reaction steps for (a) CoO_2, (b) FeO_2, (c) VSe_2 and (d) VTe_2 monolayers under different biaxial tensile strains. The PDSs are circled by dash lines and the optimal strains for the lowest overpotentials are marked by arrows.

strain, the PDSs of the OER on monolayer CoO_2 are all the first step ΔG_1 in the absence or presence of biaxial tensile strain. For monolayer FeO_2, the PDSs of the OER are the first step ΔG_1 before the biaxial strain is lower than 3% but become the third step ΔG_3 under larger biaxial strain values. The PDSs of the OER on monolayer VSe_2 and VTe_2 are the third step ΔG_3 without any strain or in the presence of biaxial tensile strain but become the fourth step ΔG_4 (*OOH → O_2) when the strain is larger than 6% and 5%, respectively. The tensile strain imposes a significant modification and change on the PDSs of the OER, which could be used accordingly to decrease the overpotentials of the magnetic 2D monolayers.

Moreover, the relationship between biaxial tensile strain and the binding energies of the intermediates on monolayer CoO_2 is shown in Fig. 4(a). The variation in the binding energies is non-monotonic with biaxial tensile strain ε_{xy}. Under 4.0% biaxial tensile strain, the binding energies of all the intermediates decrease to their lowest, indicating the strongest binding between the intermediates and the CoO_2 surface. On the other hand, it can be seen from Fig. 4(b) that the binding energies ΔE_{O^*} and ΔE_{OOH^*} obtained under different biaxial tensile strain are approximately linear functions of ΔE_{OH^*}. The scaling relation between ΔE_{O^*} or ΔE_{OOH^*} with ΔE_{OH^*} is fitted as $\Delta E_{O^*} = 0.70462 \times \Delta E_{OH^*} + 2.26156$ or $\Delta E_{OOH^*} = 0.59148 \times \Delta E_{OH^*} + 3.5054$. Furthermore, the variation in the Gibbs free energies of the adsorbed intermediates under different biaxial tensile strain values shown in Fig. 4(c) is similar to that of the binding energies. There still exists approximately linear scaling relations between G_{O^*} or G_{OOH^*} with G_{OH^*}: $G_{O^*} = 0.69712 \times G_{OH^*} + 2.0999$ and $G_{OOH^*} = 0.53982 \times G_{OH^*} + 3.79849$, see Fig. 4(d). As a result, ΔE_{OH^*} and G_{OH^*} can be used to predict the binding energies and Gibbs free energies of the *O and *OOH intermediates on the CoO_2 surface. For the FeO_2, VSe_2 and VTe_2 monolayers, their Gibbs free energies G_{O^*} and G_{OOH^*} under different biaxial tensile strain also exhibit approximately linear relations with G_{OH^*}, see Fig. S1 and S2 (ESI†). These linear scaling relations between ΔE_{O^*} or ΔE_{OOH^*} with ΔE_{OH^*} and between G_{O^*} or G_{OOH^*} with G_{OH^*} are consistent with previous studies.[44,45,48,49,51]

The metal atoms of 2D materials play a key catalytic role in the OER and HER.[50,51] To reveal the mechanism of tensile strain that modifies the catalytic properties of the metal atoms, Fig. 5 shows the density of states (DOS) of the metal atoms (Co, Fe and V) of the CoO_2, FeO_2, VSe_2 and VTe_2 monolayers without strain and under the biaxial tensile strain that leads to

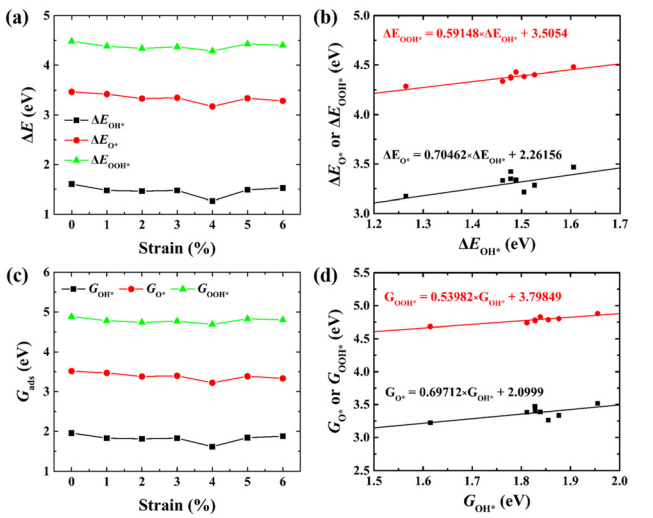

Fig. 4 (a) Binding energies of the three intermediates on the CoO_2 monolayer under different biaxial tensile strain, and (b) the scaling relation between ΔE_{OH^*} and ΔE_{O^*} or ΔE_{OOH^*}. (c) Adsorption Gibbs free energies of the three intermediates on CoO_2 under different biaxial tensile strain, and (d) the scaling relations between G_{OH^*} and G_{O^*} or G_{OOH^*}. The solid lines in (b) and (d) are fitting lines.

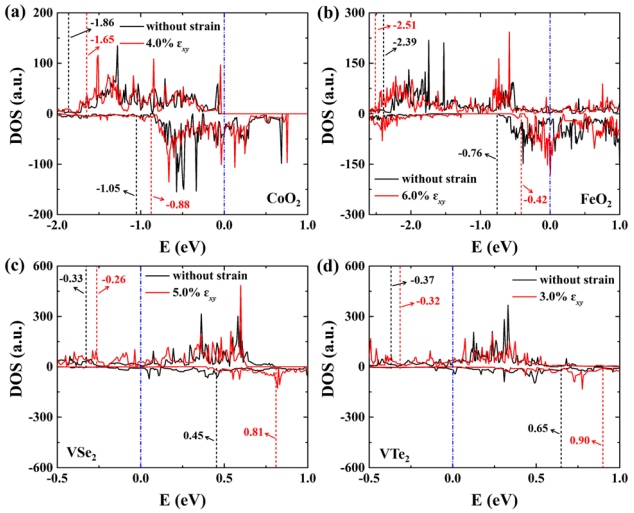

Fig. 5 DOS (in units of a.u.) of spin-up (top) and spin-down (bottom) for the metal atoms (Co, Fe and V) of (a) CoO_2, (b) FeO_2, (c) VSe_2 and (d) VTe_2 monolayers without strain and under the biaxial tensile strain that leads to the lowest overpotential. Here, the red and black dashed lines denote the d-band centers of spin-up and spin-down for the metal atoms, and the Fermi level is set to zero.

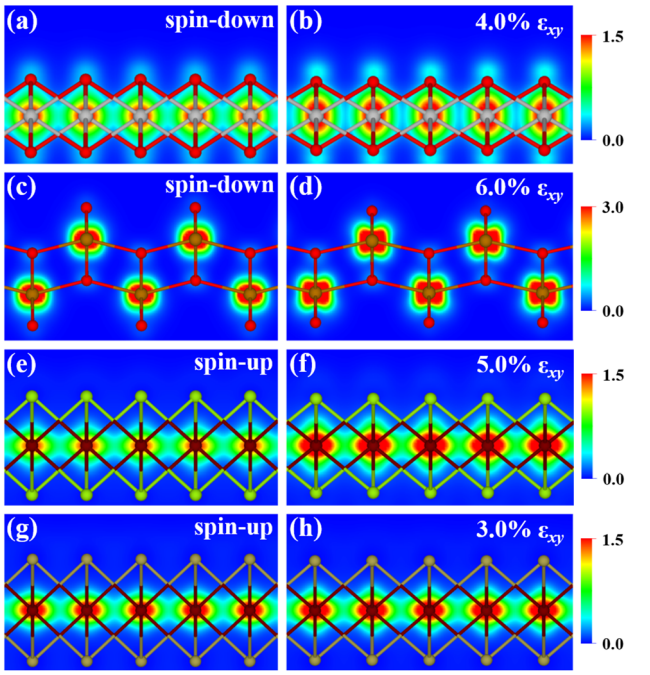

Fig. 6 2D projections of the charge densities (in units of $e{\cdot}Å^{-3}$) of (a and b) spin-down for monolayer CoO_2 in the energy range from −0.15 to 0.15 eV, (b and c) spin-down for monolayer FeO_2 in the energy range from −0.30 to 0.30 eV, (e and f) spin-up for monolayer VSe_2 in the energy range from −0.30 to 0.30 eV, and (g and h) spin-up for monolayer VTe_2 in the energy range from −0.20 to 0.20 eV in the absence and presence of biaxial tensile strain.

the lowest overpotential. It is shown from Fig. 5(a) and (b) that the DOS around the Fermi level of both spin-up and spin-down for the Co and Fe atoms is increased by the biaxial tensile strain, but the increasing magnitude of spin-down for the Fe atom is much higher than that of its spin-up counterpart. For the VSe_2 and VTe_2 monolayers, the DOS around the Fermi level of only spin-up for the V atoms is increased by the biaxial tensile strain, as shown in Fig. 5(c) and (d). Moreover, the d-band centers ε_d of the metal atoms of the four magnetic monolayers were calculated using $\varepsilon_d = \frac{\int_{-\infty}^{\infty} n_d(\varepsilon)\varepsilon\, d\varepsilon}{\int_{-\infty}^{\infty} n_d(\varepsilon) d\varepsilon}$, where $n_d(\varepsilon)$ is the density of states projected onto the d-states and ε is the energy.[52,53] The closer the d-band center is to the Fermi level, the stronger the binding with the intermediates and the better chemical activity of the metal atom.[54] For the CoO_2 and FeO_2 monolayers, biaxial tensile strain makes the d-band centers for spin-down of the metal atoms closer to the Fermi level, where the d-band center of the Co atom moves from −1.05 to −0.88 eV, and that for the Fe atom moves from −0.76 to −0.42 eV. By contrast, the d-band centers for spin-up of the V atoms for VSe_2 and VTe_2 monolayers are closer to the Fermi level when under biaxial tensile strain, where the d-band center of the V atom of VSe_2 moves from −0.33 to −0.26 eV, and that of VTe_2 moves from −0.37 to −0.32 eV. The tensile strain imposes a stronger improvement on the spin-down d-band centers of Co and Fe atoms, and on the spin-up d-band centers of V atoms. Furthermore, the spin-down charge densities $\rho_{spin\text{-}down}$ around the Fermi level of the CoO_2 and FeO_2 monolayers and the spin-up charge densities $\rho_{spin\text{-}up}$ around the Fermi level of the VSe_2 and VTe_2 monolayers are shown in Fig. 6. Clearly, more charges move to the metal atoms in the presence of biaxial tensile strain, which indicates the chemical activity enhancement of metal atoms and also coincides with the movement of the d-band centers to the Fermi level.

Different from the metal atoms, the changes in the DOS around the Fermi level of non-metal atoms (O, Se and Te) of the CoO_2, FeO_2, VSe_2 and VTe_2 monolayers are relatively slight under tensile strain, as shown in Fig. S3 (ESI†). We compared the influence of uniaxial tensile strain (in the x or y direction) on the overpotential with that of biaxial tensile strain. It can be seen from the overpotentials of the CoO_2 or VTe_2 monolayers in Fig. S4 (ESI†) that the lowest overpotentials occur under biaxial tensile strain. Furthermore, the overpotentials of four of the 2D magnetic monolayers (CoO_2, FeO_2, VSe_2 and VTe_2) were calculated using the PBE+U method.[55] As shown in Fig. S5 (ESI†), the difference in the obtained overpotentials between the PBE and PBE+U methods is slight. For comparison with the 2D magnetic monolayers, three 2D non-magnetic monolayers NiO_2, $MoTe_2$ and $MoSe_2$ were considered as catalysts for the OER using the same DFT calculation procedure. It can be seen from Fig. S6–S8 (ESI†) that the non-magnetic NiO_2, $MoSe_2$ and $MoTe_2$ monolayers are unable to bind the OOH* intermediate, and biaxial tensile strain imposes a slight influence on the DOS around the Fermi level and the G_{ads}. Clearly, the strain-induced improvement in catalytic capability of the magnetic 2D monolayers for the OER is much stronger than that for the non-magnetic 2D monolayers.

In experiments, utilizing interfacial lattice mismatch,[56,57] elastic modulus mismatch[58,59] and thermal expansion mismatch[60–62]

between the 2D materials and the substrates, as well as bending of the underlying substrates, are feasible ways to apply strain to 2D materials.[63,64] Using thermal expansion mismatch between 2D materials and substrates of high Young's modulus can generate homogenous biaxial strain on 2D materials.[60–62] In our work, the DFT results on the catalytic activity of magnetic 2D monolayers are all obtained from the homogenous tensile deformation of 2D monolayers. Therefore, in a practical situation it is better to apply homogenous strain on magnetic 2D monolayers for improving their catalytic activity for the OER.

Conclusions

In summary, our extensive first-principles calculations show that 8 magnetic 2D monolayers (CoO_2, FeO_2, FeSe, FeTe, VS_2, VSe_2, VTe_2 and $CrSe_2$) screened from 56 predicted magnetic 2D monolayers can bind O*, OH* and OOH* intermediates that are involved in the OER. The overpotentials of the CoO_2, FeO_2, VSe_2 and Vte_2 monolayers for the OER can be reduced to lower than 1.0 V by applying a suitable biaxial tensile strain. In particular, the overpotentials of the CoO_2 and VTe_2 monolayers decrease to 0.372 V and 0.491 V under biaxial tensile strain values of 4.0% and 3.0%, respectively, which are comparable to the reported overpotentials of low-dimensional materials. The reduction of overpotentials is attributed to the tensile-strain-induced modification of the PDSs and adsorption strengthening of the intermediates. Tensile strain could improve the catalytic activity of metal atoms of magnetic 2D monolayers by increasing the charge distribution around the metal atoms and moving the d-band centers of metal atoms closer to the Fermi level. These results provide a possible route for utilizing strain engineering to activate magnetic 2D monolayers as catalysts for the OER.

Conflicts of interest

There are no conflicts to declare.

Acknowledgements

This work is supported by the National Natural Science Foundation of China (11972186, 11890674, and 51921003), and the Western Light Project of CAS (xbzg-zdsys-202118), a Project Funded by the Priority Academic Program Development of Jiangsu Higher Education Institutions.

References

1 I. Roger, M. A. Shipman and M. D. Symes, *Nat. Rev. Chem.*, 2017, **1**, 0003.
2 E. Antolini, *ACS Catal.*, 2014, **4**, 1426–1440.
3 Y. C. Lu, Z. C. Xu, H. A. Gasteiger, S. Chen, K. Hamad-Schifferli and Y. Shao-Horn, *J. Am. Chem. Soc.*, 2010, **132**, 12170–12171.
4 Z. W. Seh, J. Kibsgaard, C. F. Dickens, I. B. Chorkendorff, J. K. Nørskov and T. F. Jaramillo, *Science*, 2017, **355**, 1–12.
5 M. S. Dresselhaus and I. L. Thomas, *Nature*, 2001, **414**, 332–337.
6 S. Chu, Y. Cui and N. Liu, *Nat. Mater.*, 2016, **16**, 16–22.
7 N. T. Suen, S. F. Hung, Q. Quan, N. Zhang, Y. J. Xu and H. M. Chen, *Chem. Soc. Rev.*, 2017, **46**, 337–365.
8 M. Tahir, L. Pan, F. Idrees, X. W. Zhang, L. Wang, J. J. Zou and Z. L. Wang, *Nano Energy*, 2017, **37**, 136–157.
9 J. Suntivich, K. J. May, H. A. Gasteiger, J. B. Goodenough and Y. Shao-Horn, *Science*, 2011, **334**, 1383–1385.
10 S. M. Alia, S. Shulda, C. Ngo, S. Pylypenko and B. S. Pivovar, *ACS Catal.*, 2018, **8**, 2111–2120.
11 T. Reier, M. Oezaslan and P. Strasser, *ACS Catal.*, 2012, **2**, 1765–1772.
12 J. T. Zhang, Z. H. Zhao, Z. H. Xia and L. M. Dai, *Nat. Nanotechnol.*, 2015, **10**, 444–452.
13 D. J. Akinwande, C. J. Brennan, J. S. Bunch, P. Egberts, J. R. Felts, H. J. Gao, R. Huang, J. S. Kim, T. Li, Y. Li, K. M. Liechti, N. S. Lu, H. S. Park, E. J. Reed, P. Wang, B. I. Yakobson, T. Zhang, Y. W. Zhang, Y. Zhou and Y. Zhu, *Ext. Mech. Lett.*, 2017, **13**, 42–77.
14 D. Jariwala, V. K. Sangwan, L. J. Lauhon, T. J. Marks and M. C. Hersam, *ACS Nano*, 2014, **8**, 1102–1120.
15 B. You, M. T. Tang, C. Tsai, F. Abild-Pedersen, X. L. Zheng and H. Li, *Adv. Mater.*, 2019, **31**, 1807001.
16 Y. N. Guo, T. Park, J. W. Yi, J. Henzie, J. Kim, Z. L. Wang, B. Jiang, Y. Bando, Y. Sugahara, J. Tang and Y. Yamauchi, *Adv. Mater.*, 2019, **31**, 1807134.
17 Y. J. Ji, M. Y. Yang, H. P. Lin, T. J. Hou, L. Wang, Y. Y. Li and S. T. Lee, *J. Phys. Chem. C*, 2018, **122**, 3123–3129.
18 H. Li, C. Tsai, A. L. Koh, L. L. Cai, A. W. Contryman, A. H. Fragapane, J. H. Zhao, H. S. Han, H. C. Manoharan, F. Abild-Pedersen, J. K. Nørskov and X. L. Zheng, *Nat. Mater.*, 2016, **15**, 48–53.
19 T. Yang, J. Zhou, T. T. Song, L. Shen, Y. P. Feng and M. Yang, *ACS Energy Lett.*, 2020, **5**, 2313–2321.
20 J. F. Xie, J. J. Zhang, S. Li, F. Grote, X. D. Zhang, H. Zhang, R. X. Wang, Y. Lei, B. C. Pan and Y. Xie, *J. Am. Chem. Soc.*, 2013, **135**, 17881–17888.
21 C. L. Wang, H. G. Tong, J. Lu, B. Liu, F. C. Zheng, W. W. Tao, W. J. Zhang and Q. W. Chen, *Carbon*, 2020, **170**, 414–420.
22 G. T. Hai, H. Y. Gao, G. X. Zhao, W. J. Dong, X. B. Huang, Y. Li and G. Wang, *iScience*, 2019, **20**, 481–488.
23 G. Murdachaew and K. Laasonen, *J. Phys. Chem. C*, 2018, **122**, 25882–25892.
24 E. German and R. Gebauer, *Appl. Surf. Sci.*, 2020, **528**, 146591.
25 H. L. Fei, J. C. Dong, Y. X. Feng, C. S. Allen, C. Z. Wan, B. Volosskiy, M. F. Li, Z. P. Zhao, Y. L. Wang, H. T. Sun, P. F. An, W. X. Chen, Z. Y. Guo, C. Lee, D. L. Chen, I. Shakir, M. J. Liu, T. D. Hu, Y. D. Li, A. I. Kirkland, X. F. Duan and Y. Huang, *Nat. Catal.*, 2018, **1**, 63–72.
26 J. Q. Guan, Z. Y. Duan, F. X. Zhang, S. D. Kelly, R. Si, M. Dupuis, Q. G. Huang, J. Q. Chen, C. H. Tang and C. Li, *Nat. Catal.*, 2018, **1**, 870–877.
27 H. J. Lee, S. Back, J. H. Lee, S. H. Choi, Y. Jung and J. W. Choi, *ACS Catal.*, 2019, **9**, 7099–7108.
28 B. S. Tang, Z. G. Yu, H. L. Seng, N. D. Zhang, X. X. Liu, Y. W. Zhang, W. F. Yang and H. Gong, *Nanoscale*, 2018, **10**, 20113–20119.

29 O. Gutfleisch, M. A. Willard, E. Bruck, C. H. Chen, S. G. Sankar and J. P. Liu, *Adv. Mater.*, 2011, **23**, 821–842.
30 Z. R. Xiong, C. Hu, X. F. Luo, W. D. Zhou, Z. Z. Jiang, Y. Yang, T. Yu, W. Lei and C. L. Yuan, *Nano Lett.*, 2021, **21**, 10486–10493.
31 X. M. Hu, S. L. Zhang, J. W. Sun, L. Yu, X. Y. Qian, R. D. Hu, Y. N. Wang, H. G. Zhao and J. W. Zhu, *Nano Energy*, 2019, **56**, 109–117.
32 C. L. Qin, A. X. Fan, X. Zhang, S. Q. Wang, X. L. Yuan and X. P. Dai, *J. Mater. Chem. A*, 2019, **7**, 27594–27602.
33 S. Q. Zhang, R. Z. Xu, N. N. Luo and X. L. Zou, *Nanoscale*, 2021, **13**, 1398–1424.
34 M. Gibertini, M. Koperski, A. F. Morpurgo and K. S. Novoselov, *Nat. Nanotechnol.*, 2019, **14**, 408–419.
35 N. Mounet, M. Gibertini, P. Schwaller, D. Campi, A. Merkys, A. Marrazzo, T. Sohier, I. E. Castelli, A. Cepellotti, G. Pizzi and N. Marzari, *Nat. Nanotechnol.*, 2018, **13**, 246.
36 H. Y. Jin, C. X. Guo, X. Liu, J. L. Liu, A. Vasileff, Y. Jiao, Y. Zheng and S. Z. Qiao, *Chem. Rev.*, 2018, **118**, 6337–6408.
37 P. F. Li, Z. Kang, Z. Zhang, Q. L. Liao, F. Rao, Y. Lu and Y. Zhang, *Mater. Today*, 2021, **51**, 247–272.
38 B. Huang, G. Clark, E. Navarro-Moratalla, D. R. Klein, R. Cheng, K. L. Seyler, D. Zhong, E. Schmidgall, M. A. McGuire, D. H. Cobden, W. Yao, D. Xiao, P. Jarillo-Herrero and X. D. Xu, *Nature*, 2017, **546**, 270.
39 C. Gong, L. Li, Z. L. Li, H. W. Ji, A. Stern, Y. Xia, T. Cao, W. Bao, C. Z. Wang, Y. Wang, Z. Q. Qiu, R. J. Cava, S. G. Louie, J. Xia and X. Zhang, *Nature*, 2017, **546**, 265.
40 G. Kresse and J. Furthmüller, *Phys. Rev. B: Condens. Matter Mater. Phys.*, 1996, **54**, 11169–11186.
41 P. E. Blöchl, *Phys. Rev. B: Condens. Matter Mater. Phys.*, 1994, **50**, 17953–17979.
42 J. P. Perdew, K. Burke and M. Ernzerhof, *Phys. Rev. Lett.*, 1996, **77**, 3865–3868.
43 S. Grimme, J. Antony, S. Ehrlich and H. Krieg, *J. Chem. Phys.*, 2010, **132**, 154104.
44 J. Rossmeisl, Z. W. Qu, H. Zhu, G. J. Kroes and J. K. Nørskov, *J. Electroanal. Chem.*, 2007, **607**, 83–89.
45 I. C. Man, H. Y. Su, F. Calle-Vallejo, H. A. Hansen, J. I. Martínez, N. G. Inoglu, J. Kitchin, T. F. Jaramillo, J. K. Nørskov and J. Rossmeisl, *ChemCatChem*, 2011, **3**, 1159–1165.
46 J. K. Nørskov, J. Rossmeisl, A. Logadottir, L. Lindqvist, J. R. Kitchin, T. Bligaard and H. Jónsson, *J. Phys. Chem. B*, 2004, **108**, 17886–17892.
47 X. F. Liu, Y. F. Zhang, W. T. Wang, Y. Z. Chen, W. J. Xiao, T. Y. Liu, Z. Zhong, Z. J. Luo, Z. Ding and Z. F. Zhang, *ACS Appl. Mater. Interfaces*, 2022, **14**, 1249–1259.
48 S. Lu, Y. Zhang, F. L. Lou, K. Guo and Z. X. Yu, *Appl. Surf. Sci.*, 2022, **579**, 152234.
49 M. T. Li, L. P. Zhang, Q. Xu, J. B. Niu and Z. H. Xia, *J. Catal.*, 2014, **314**, 66–72.
50 X. Chen, H. Zhang and Y. Z. Zhang, *Colloids Surf., A*, 2021, **630**, 127628.
51 X. P. Xu, H. X. Xu and D. J. Cheng, *Nanoscale*, 2019, **11**, 20228–20237.
52 B. Hammer and J. K. Nørskov, *Nature*, 1995, **376**, 238–240.
53 B. Hammer and J. K. Nørskov, *Surf. Sci.*, 1995, **343**, 211–220.
54 A. Ruban, B. Hammer, P. Stoltze, H. L. Skriver and J. K. Nørskov, *J. Mol. Catal. A: Chem.*, 1997, **115**, 421–429.
55 L. Wang, T. Maxisch and G. Ceder, *Phys. Rev. B: Condens. Matter Mater. Phys.*, 2006, **73**, 195107.
56 M. Y. Li, Y. M. Shi, C. C. Cheng, L. S. Lu, Y. C. Lin, H. L. Tang, M. L. Tsai, C. W. Chu, K. H. Wei, J. H. He, W. H. Chang, K. Suenaga and L. J. Li, *Science*, 2015, **349**, 524–528.
57 C. D. Zhang, M. Y. Li, J. Tersoff, Y. M. Han, Y. S. Su, L. J. Li, D. A. Muller and C. K. Shih, *Nat. Nanotechnol.*, 2018, **13**, 152–158.
58 K. P. Dhakal, S. Roy, H. Jang, X. Chen, W. S. Yun, H. Kim, J. Lee, J. Kim and J. H. Ahn, *Chem. Mater.*, 2017, **29**, 5124–5133.
59 S. X. Yang, C. Wang, H. Sahin, H. Chen, Y. Li, S. S. Li, A. Suslu, F. M. Peeters, Q. Liu, J. B. Li and S. Tongay, *Nano Lett.*, 2015, **15**, 1660–1666.
60 G. Plechinger, A. Castellanos-Gomez, M. Buscema, H. S. J. van der Zant, G. A. Steele, A. Kuc, T. Heine, C. Schuller and T. Korn, *2D Mater.*, 2015, **2**, 015006.
61 P. Gant, P. Huang, D. P. de Lara, D. Guo, R. Frisenda and A. Castellanos-Gomez, *Mater. Today*, 2019, **27**, 8–13.
62 G. H. Ahn, M. Amani, H. Rasool, D. H. Lien, J. P. Mastandrea, J. W. Ager, M. Dubey, D. C. Chrzan, A. M. Minor and A. Javey, *Nat. Commun.*, 2017, **8**, 608.
63 C. R. Zhu, G. Wang, B. L. Liu, X. Marie, X. F. Qiao, X. Zhang, X. X. Wu, H. Fan, P. H. Tan, T. Amand and B. Urbaszek, *Phys. Rev. B: Condens. Matter Mater. Phys.*, 2013, **88**, 121301.
64 Z. W. Li, Y. W. Lv, L. W. Ren, J. Li, L. A. Kong, Y. J. Zeng, Q. Y. Tao, R. X. Wu, H. F. Ma, B. Zhao, D. Wang, W. Q. Dang, K. Q. Chen, L. Liao, X. D. Duan, X. F. Duan and Y. Liu, *Nat. Commun.*, 2020, **11**, 1151.

